Title
DIRECT OBSERVATION OF LIQUID-PHASE SINTERING IN THE SYSTEM IRON-COPPER

Authors
Froschauer, Leonhard
Fulrath, Richard M.

Publication Date
1974-06-01

Submitted to Journal of Materials Science

LBL-2770
Preprint

DIRECT OBSERVATION OF LIQUID-PHASE SINTERING IN THE SYSTEM IRON-COPPER

Leonhard Froschauer and Richard M. Fulrath

June, 1974

Prepared for the U. S. Atomic Energy Commission
under Contract W-7405-ENG-48

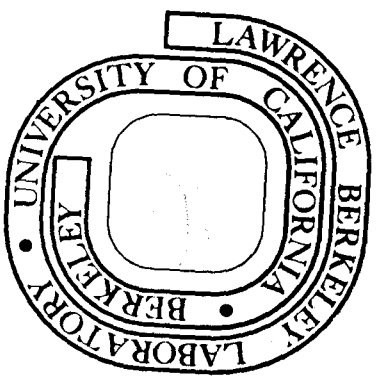

DISCLAIMER

DIRECT OBSERVATION OF LIQUID-PHASE SINTERING IN THE SYSTEM IRON-COPPER

Leonhard Froschauer and Richard M. Fulrath

Inorganic Materials Research Division, Lawrence Berkeley Laboratory
and Department of Materials Science and Engineering,
College of Engineering; University of California,
Berkeley, California 94720

SYNOPSIS

The hot-stage of a scanning electron microscope has been used to observe liquid-phase sintering in the system iron-copper. Densification behavior and mechanism of samples with spherical Fe and Cu particles have been determined, the influence of the particle sizes of both components and the amount of liquid phase in this system have been investigated. In samples with about 20% liquid phase, the densification kinetics is that of a rearrangement process; the direct observation proves that no rearrangement takes place. In samples with 40% liquid phase and particle sizes of 10-20 μm, some rearrangement can be found.

1. INTRODUCTION

Liquid-phase sintering, i.e. sintering where a proportion of the material being sintered is in the liquid state, is a common processing technique for a variety of systems, including metal compositions, cermets, and ceramics. The sintered material usually consists of grains of one or more phases dispersed in a matrix that is liquid at sintering temperature.

It is very important to understand the properties of the system that control the densification behavior and the optical microstructure (grain size and shape, pore size and shape) because of their effect on

the properties of the final product. This understanding is complicated mainly by three reasons:

(a) The existence of at least three phases at sintering temperature (solid, liquid, vapor) increases the number of parameters (esp. boundary energies between single phases, solubilities, quantities).

(b) Changing boundary energies and solubilities can change the microstructure during the cooling of the system to room temperature, where the microstructure normally is observed.

(c) The often very fast shrinkage after the first appearance of the liquid phase makes it extremely difficult to stop the densification in different states of the process.

For these reasons, most research work has followed this scheme:

(a) Determination of sintering behavior (densification, microstructure) and qualitative explanation of the results, using known properties of the system.

(b) Model calculations for possible densification processes and conclusion on the actual mechanism by comparison with the measured densification kinetics.

The availability of a hot stage for the scanning electron microscope (SEM) allowed a new approach to the problems. Direct observation of the sintering has been tried before by hot-stage microscopy [1,2] but the low depth of field makes it complicated. The hot stage of the SEM provides a means for continuous monitoring and filming of the microstructure during the sintering process. This allows more detailed conclusions on mechanisms.

2. GENERAL BACKGROUND

Sintering studies have been performed for many materials, a review article by EREMENKO et al. [3] gives detailed description of the results. The main properties of the components and the system that influence the sintering behavior have been listed in Table I.

Tables II and III give the proposed sintering mechanisms and the corresponding kinetics that result from model calculations. A description of these mechanisms can be found in review articles (for example [9]) or in the original literature.

For the application of the SEM hot stage, it was intended to use systems with a model character that have been investigated previously. Three systems, Fe-Cu, WC-Co, and W-Cu have been chosen; the main properties (for sintering) of these systems are listed in Table IV. This first part deals with the results for Fe-Cu.

The system Fe-Cu has been often investigated and is of special interest both from a theoretical and practical point of view.

CANNON [10], KINGERY [11], and RAMAKRISHNAN [12] find during the first minutes a time-proportional shrinkage. Kingery used this system to prove the existence of a rearrangement process in the early stages of densification, for which his theory predicted

$$\Delta L/L_o \sim t^{1+y} \quad (y<<1)$$

This densification mechanism seems to be widely accepted for Fe-Cu [9], in spite of the fact that the properties of the system do not meet the requirements of Kingery's model. He assumes complete wetting of the two

phases with a dihedral angle of 0°, so that the liquid penetrates into the gaps between iron particles. The dihedral angle in this system, however, has been measured as 27° (Table IV). Following this fast densification, a second stage is reported in which a dependence

$$\Delta L/L_o \sim t^{1/3}$$

seems to describe the results. Again referring to Kingery's models, a solution-precipitation process is assumed. But there again the model uses the assumption of zero dihedral angle that leads to no particle-particle contacts. Microstructure observations showed strong neckgrowth in very short times and a very fast particle growth. WHALEN and HUMENIK [13] report that within 20 minutes the average particle size changes from 10 µm to 30 µm.

3. EXPERIMENTAL PROCEDURE

3.1 Sample Preparation

The starting powders were spherical iron and copper that were sieved into different size fractions. The used fractions were 10 to 20 µm and <37 µm for iron, 10 to 20 µm and <44 µm for copper. Mixtures of the powders were prepared with 10 to 50 vol% copper and mixed in alcohol for 24 hours.

Samples with 3/16 inch diameter were cold-pressed with about 200 MN/m^2, this resulted in green densities of about 70%. To remove oxide films from the surfaces, all samples were prefired for one hour at 450°C in helium-4% hydrogen.

3.2 Sintering

The sintering was carried out in vacuum in the hot stage of a scanning microscope. An older design of the hot stage has been described previously [14]; Figure 1 shows the new specimen stage used in this experiment. This stage can reach temperatures up to 1700°C. The sample rests in a molybdenum cup inside the heating element. The temperature was determined with a thermocouple welded to the bottom of a flat stand for the cup. For shrinkage measurements, the SEM was operated at low magnifications of about 100X; alumina spheres on the sample surface served as markers to determine the shrinkage. Figure 2 shows a sample surface during sintering with marker spheres.

The screen of a TV set can be filmed with a camera that allowed continuous framing with speeds of 1 to .1 frames/second. The distances between the markers are measured from the film. For the observation of microstructure, the SEM can be operated at magnifications up to 5000X.

For all samples, the same heating cycle has been used. The material was heated to 900°C in 4 minutes, held isothermally for 5 minutes, and was then heated at 7.8°C/min. to 1135°C. Then the samples were held for 45 minutes at this temperature.

4. RESULTS AND DISCUSSION

4.1 Shrinkage

To find the influence of different parameters (content of liquid phase, particle size of both components), a series of experiments was performed. Figures 3 to 6 show densification results for samples with different combinations of particle sizes.

In all cases the densification rate increases with increasing liquid content. This is in accordance with all proposed mechanisms, because rearrangement (due to fewer contact points between Fe-Fe particles) diffusion and solution-controlled processes are enhanced by increasing liquid phase content. (The very few exceptions from this behavior are in systems with a high solubility of the liquid in the solid phase.)

The increase in densification with decreasing solid-phase particle size (Fig. 7) is also expected by the models. Smaller particles (of the same shape) have higher mobilities (for rearrangement) and need less material transport for solution-precipitation.

The influence of the size of the liquid forming particles (Fig. 7) has not been reported previously. This effect can be explained as follows:

After melting, the liquid phase is distributed in the compact of iron particles. In equilibrium, the small pores will be filled with liquid phase and the large pores will be open, because the capillary forces increase with 1/r with decreasing pore radius. For large liquid forming particles, their size determines the largest pore size, the main pores in the compact are the spaces previously held by Cu particles.

This can be seen in micrographs. Figure 8 shows polished sections of different samples after sintering for 45 minutes. Even after this long time, the pores are roughly of the size of the molten particles. Figure 9 shows samples of 80 Fe-20 Cu (both 10-20 μm) in different states of the process. Between 9a and 9b the copper melted, the small pores in 9a have filled with Cu and large pores have opened; their size corresponds to the Cu-particle size. After 45 minutes sintering (9d) the

large pores still are present. Remarkable is the strong particle growth after this time.

To compare with literature results and to follow the usual scheme of previous research, the results have been plotted on a log-log-scale (Fig. 10). (As time zero the time for 1100°C was chosen.)

From these plots, two essential conclusions can be drawn:

(1) The results are in general agreement with previous research.

(2) Results that show an abrupt change of slope from 1 to 1/3 cannot be verified. It seems rather reasonable to assume a change in slope in a smooth curve.

4.2 Densification Mechanism

Comparing the densification kinetics with the different models, it must be concluded that the first part of the densification is a rearrangement process, followed by a slower mechanism. For 80 Fe-20 Cu during the first 40 minutes, the whole densification follows rearrangement kinetics.

This could not be verified in direct observation. Figures 11 to 13 show SEM pictures of samples with 20 and 40 vol% Cu during the sintering process. In the samples with 20% Cu, no sign of a change of the relative positions of the iron spheres can be found; in samples with 40% Cu (particle size 10-20 µm) some relative movement takes place (Fig. 13). This can be seen better in a continuous film.

Another result that strongly contradicts a rearrangement process is the neckgrowth during the heating of the samples to the melting temperature (Fig. 9a). After melting the liquid phase does not penetrate into

these necks. This behavior can be predicted theoretically for a system with a dihedral angle of nearly 30° and can be confirmed in micrographs (Fig. 9b, 9c). For higher amounts of liquid phase, the number of solid neighbors and thus the probability for the formation of a rigid skeleton decreases.

The hot-stage observations and the micrographs seem to prove that the densification in this system (liquid content 20%) is completely by a diffusion process. No rearrangement can be found, and the strong particle growth and change of particle shape corresponding to the shape of the neighbors (see Fig. 9d) are hints for a solution-precipitation process. The change in particle shape to give a close packing makes a process similar to that proposed by Kingery [5] probable. He assumed that near contact points the chemical potential and thus the solubility are increased due to stresses originated by the capillary forces.

This result allows the conclusions that it is not possible to find the densification mechanism in a non-complete wetting system by comparing the sintering kinetics with the results of existing model calculations. The main reason for the different behavior seems to be that even in calcualtions for non-complete wetting systems, a regular array of solid spheres with uniform porosity is assumed. In real systems there is always a distribution of pore sizes and thus a distribution of the liquid phase where small pores (that would result in a large capillary pressure) are closed and large pores are open. A better fit of the model calculations can be expected where the liquid-forming phase has a very small particle size compared to the solid phase.

5. CONCLUSIONS

Direct observation of sintering processes in the hot stage of a scanning electorn microscope can give two improvements compared to conventional techniques: at low magnifications the densification can be determined even for very fast shrinking samples without the disadvantages of dilatometry, and at high magnifications the microstructure can be observed continually at sintering temperature.

The determination of liquid-phase sintering in the system Fe-Cu showed that the densification rate is in general agreement with previous results, but the continuous determination of shrinkage proved that the densification is not, as previously assumed, a process with two distinct stages and an abrupt change in the time-dependence but rather a smooth transition with continuously changing slope.

The observation of microstructure showed that in this system for lower amounts of liquid phase, no rearrangement in the early stages of densification can be found. This could be expected from earlier data on neck and particle-growth and the wetting behavior of Fe-Cu, but it contradicts the densification kinetics and its explanation by model calculations. New calculations for non-complete wetting systems regarding the actual pore-size distribution seem to be necessary.

ACKNOWLEDGMENTS

We want to thank Professor Joseph A. Pask for reviewing the manuscript and for many valuable comments.

The work was supported by the United States Atomic Energy Commission through the Inorganic Materials Research Division of the Lawrence Berkeley Laboratory and by the Deutsche Forschungsgemeinschaft.

REFERENCES

1. E. M. DAVER and W. F. ULLRICH in Perspectives of Powder Metallurgy ed. Hirschhorn and Roll, pp. 189-200.
2. N. DAUTZENBERG, Arch. Eisenhüttenwes. 41 (1970) 1005-1010.
3. V. N. EREMENKO, Yu. V. NAIDICH, I. A. LAVRINENKO, Special Report "Liquid Phase Sintering" (1970).
4. T. PRICE, C. SMITHELLS, S. WILLIAMS, J. Inst. of Met., 62 (1938) 239-269.
5. W. D. KINGERY, J. Appl. Phys. 30 (1959) 301-306.
6. B. CECH, Sov. Powder Met. (1963) 86-92.
7. C. HOGE and J. PASK, private communication.
8. G. H. GESSINGER, H. F. FISCHMEISTER, H. L. LUKAS, Acta Met. 21 (1973) 715-724.
9. T. J. WHALEN and M. HUMENIK in Sintering and Related Phenomena, ed. G. Kuczynski, pp. 715-746.
10. H. S. CANNON and F. V. LENEL, Plansee-Seminar Pulvermetallurgie 1953, pp. 106-121.
11. W. D. KINGERY and M. D. NARASIMHAN, J. Appl. Phys. 30 (1959) 307-310.
12. P. RAMAKRISHNAN and R. LAKSHMINARASIMHAN, Int. J. of Powder Met. 3 (1967) 63-72.
13. T. J. WHALEN and M. HUMENIK, Progr. in Powder Met. 18 (1962) 85-98.
14. R. M. FULRATH, 5th Annual Scanning Electron Microscopy Symposium, Chicago 1972.
15. L. RAMQUIST, Int. J. of Powder Met. 1 (4), (1965) 2-20.
16. Yu. V. NAIDICH, I. A. LAVRINENKO and V. N. EREMENKO, ibid. 1 (4) (1965) 41-48.

Table I. Main influences on liquid phase sintering

Property	Influence
Property of the solid phase	
Particle size and shape	Mobility of the particles for rearrangement. Necessary diffusion for solution-precipitation.
Properties of the liquid-forming phase	
(a) Particle size and shape (?)	Pore size after melting for large liquid-forming particles.
(b) Viscosity	Viscosity of whole sample (rearrangement). Penetration into crevices between solid particles.
Common properties	
(a) Wetting behavior (characterized by contact and dihedral angle)	Capillary forces for densification. Penetration into gaps between solid particles (rearrangement and solution-precipitation).
(b) Solubilities Liquid in solid	Amount of liquid phase changes during sintering.
Solid in liquid	Solution of necks. Solution-precipitation process.
(c) Quantities	Viscosity of sample (rearrangement). Porosity after rearrangement.
(d) Green density	Ability of solid particles to rearrange (interlocking).
(e) Relative melting points	Neck-growth of solid phase during heating. Change in apparent particle size.

Table II. Proposed sintering mechanisms and kinetics

Author	Ref.	Process	Kinetics	Assumptions
Price et al.	[4]	"heavy alloy mechanism" ≙ "Ostwald ripening"		
Kingery	[5]	rearrangement	$\Delta L/L_o \sim t^{1+y}$ $y \ll 1$	complete wetting zero dihedral angle for solution-precipitation-process solubility of solid in liquid
		solution-precipitation	(a) $\Delta L/L_o \sim r^{-4/3} t^{1/3}$ spheres	
			$\Delta L/L_o \sim t^{1/5}$ prisms	
			(b) $\sim r^{-1} t^{1/2}$ spheres	
			$\sim t^{1/3}$ prisms	
			(a) diffusion-controlled (b) solution-controlled	
Cech	[6]	viscous flow	$\Delta L/L_o = K_1 (\log t - \log t_o)$	entrapped gas in pores,
			$- K_2 (t^4 - t_K^4)$	pores close at t_K
			$+ K_3 t^{1/3}$	term 3 for gas diffusion
Hoge and Pask	[7]	solution-precipitation	see Table III	sphere model
Fischmeister et al.	[8]	solution-precipitation	time exponent .3125 to .333 changing with liquid volume, dihedral angle and shrinkage	sphere model

TABLE OF EXPONENTS

$\frac{h}{R_o} \alpha t^y R_o^z$	y	z
Zero Dihedral Angle		
Initial stage	0.243	-0.977
Combination of initial and final stage		
4.4% liquid	0.246	*
20% liquid	0.268	*
Final stage large liquid volume 34.3%		
No back pressure	0.362	-1.45
With back pressure	0.282	-1.13
Dissimilar particles		
Ratio 2:1	0.255	-1.019
5:1	0.304	-1.215
20:1	0.372	-1.488
Non Zero Dihedral Angle		
Johnson's model $\gamma_{sl}/\gamma_{lv} = 0.01$	0.437	*
$\gamma_{sl}/\gamma_{lv} = 3.00$	0.448	*
Coble's model $\gamma_{sl}/\gamma_{lv} = 1.00$	0.464	-1.390
$\gamma_{sl}/\gamma_{lv} = 3.00$	0.475	-1.425

*Not determined

Table IV. Important properties of three systems for LPS

System	$\frac{T_m \text{ (liquid)}}{T_m \text{ (solid)}}$	Contact angle		Dihedral angle		Solubility solid in liquid
Fe-Cu	.79	0° (H_2)	[9]	27°	[9]	5%
W-Cu	.37	30° 1150°C (H_2) 0° 1350°C	[16]	-		no
WC-Co	.60	0° (vac.)	[15]	probably 0° (see disc. in 9)		40%

FIGURE CAPTIONS

Fig. 1. Specimen stage of the SEM-hot stage.

Fig. 2. Sample surface with alumina marker spheres.

Figs. 3-6. Densification curves for iron-copper, different combinations of particle sizes.

Fig. 7. Densification of 70 Fe-30 Cu as a function of particle sizes.

Fig. 8. Microstructure after sintering for 45 minutes as a function of the particle sizes and the amount of liquid phase.

Fig. 9. Microstructures of samples 80 Fe-20 Cu (10-20 μm) in different states. (a) before melting, (b) immediately after melting, (c) 5 minutes after melting, (d) 45 minutes after melting.

Fig. 10. Volume shrinkage as a function of time for different samples (including literature results).

Fig. 11. SEM hot stage pictures of a sample 80 Fe-20 Cu (both 10-20 μm) in different states of the heating and sintering process.

Fig. 12. Dto. for a sample 80 Fe-20 Cu (Fe <37 μm, Cu <44 μm).

Fig. 13. Dto. for a sample 60 Fe-20 Cu (both 10-20 μm).

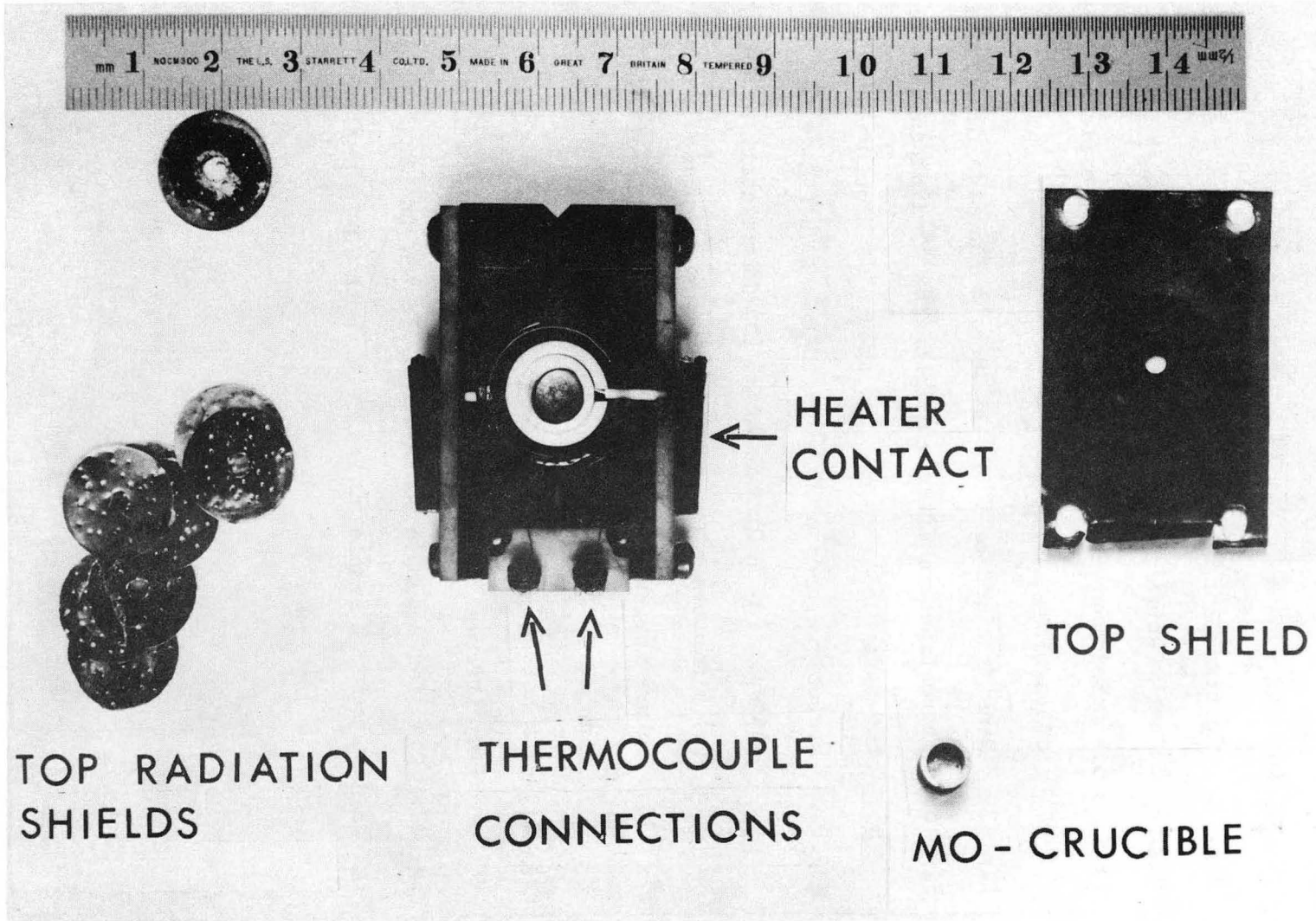

XBB 745-3466

Fig. 1

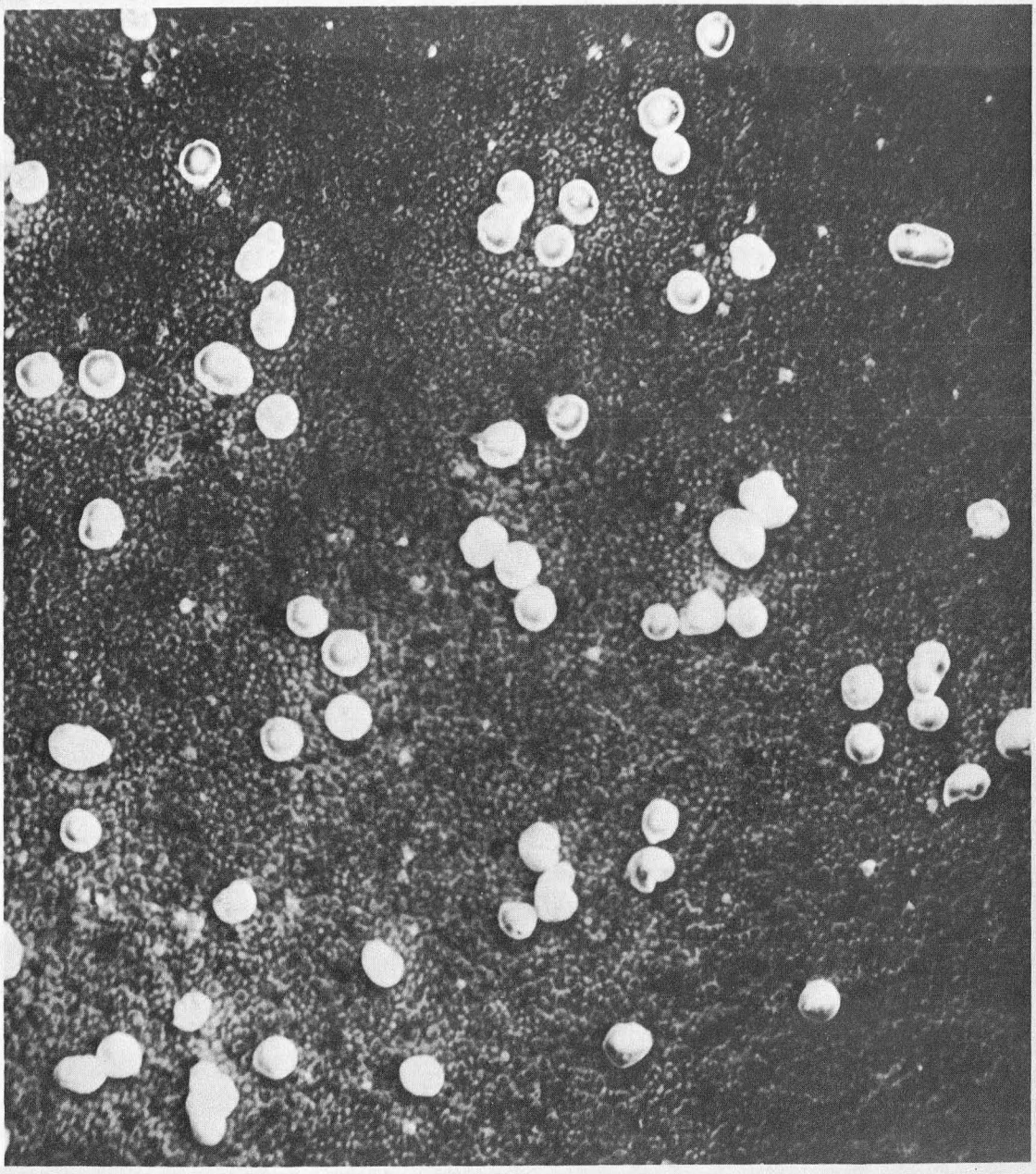

CBB748-5858

Fig. 2

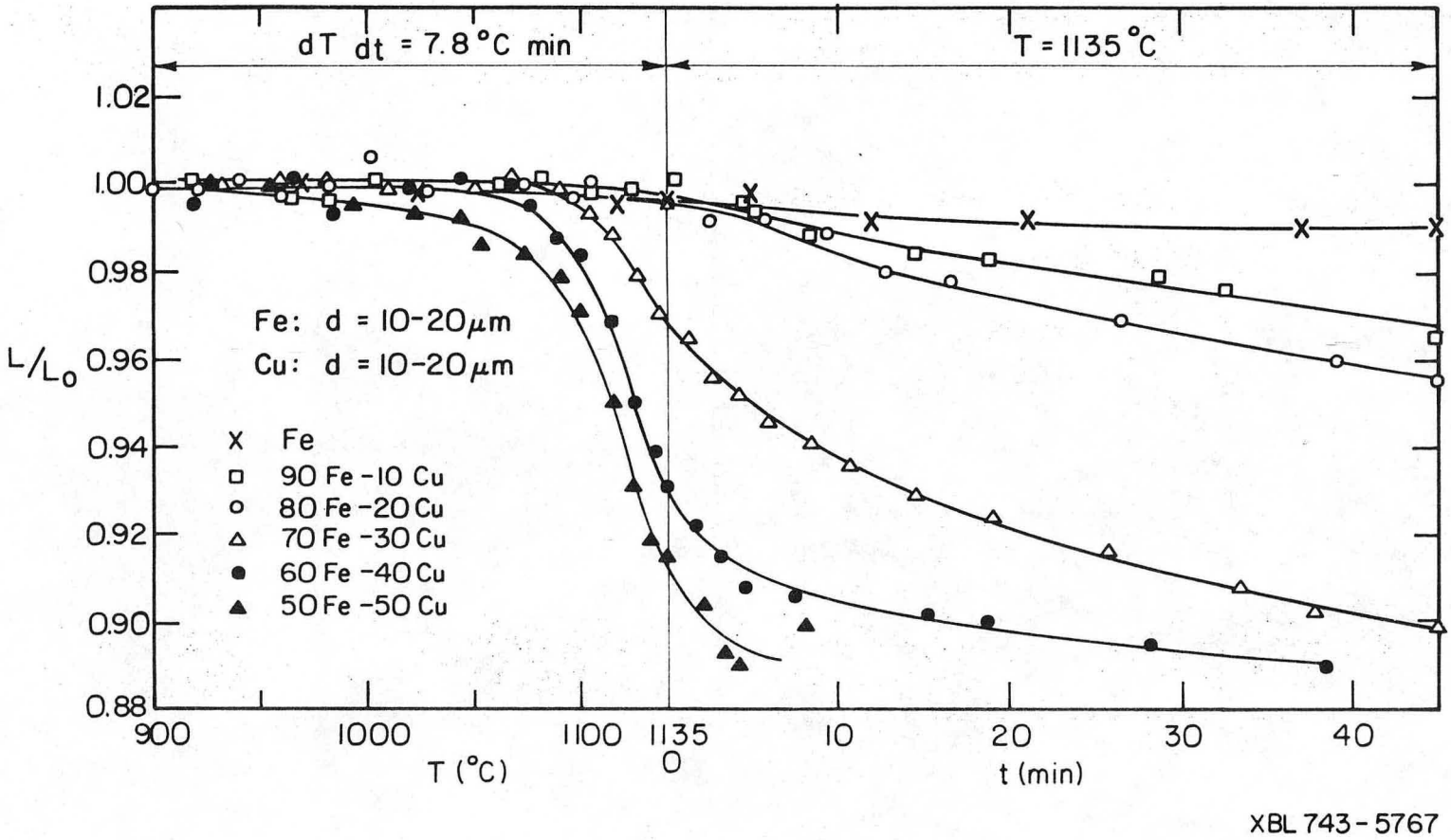
dT dt = 7.8 °C min
T = 1135 °C
1.02
1.00
0.98
0.96
0.94
0.92
0.90
0.88
L/L0
Fe: d = 10-20μm
Cu: d = 10-20μm
X Fe
□ 90 Fe -10 Cu
○ 80 Fe -20 Cu
△ 70 Fe -30 Cu
● 60 Fe -40 Cu
▲ 50 Fe -50 Cu
900
1000
1100
1135
T (°C)
0
10
20
30
40
t (min)
XBL 743-5767

Fig. 3

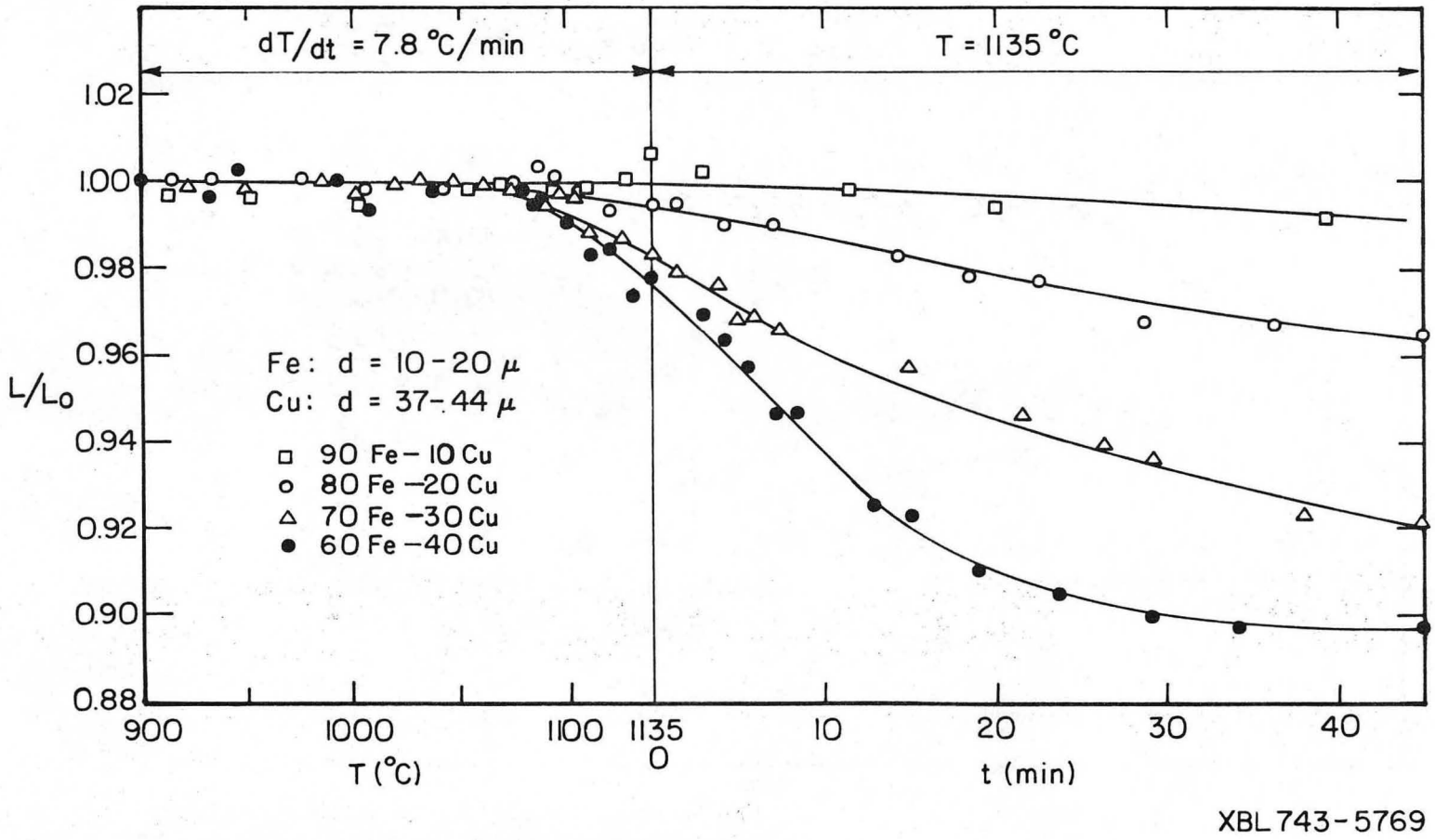
dT/dt = 7.8 °C/min
T = 1135 °C
1.02
1.00
0.98
0.96
0.94
0.92
0.90
0.88
L/Lo
Fe: d = 10-20 μ
Cu: d = 37-44 μ
90 Fe-10 Cu
80 Fe-20 Cu
70 Fe-30 Cu
60 Fe-40 Cu
900
1000
1100
1135
0
10
20
30
40
T (°C)
t (min)
XBL 743-5769

Fig. 4

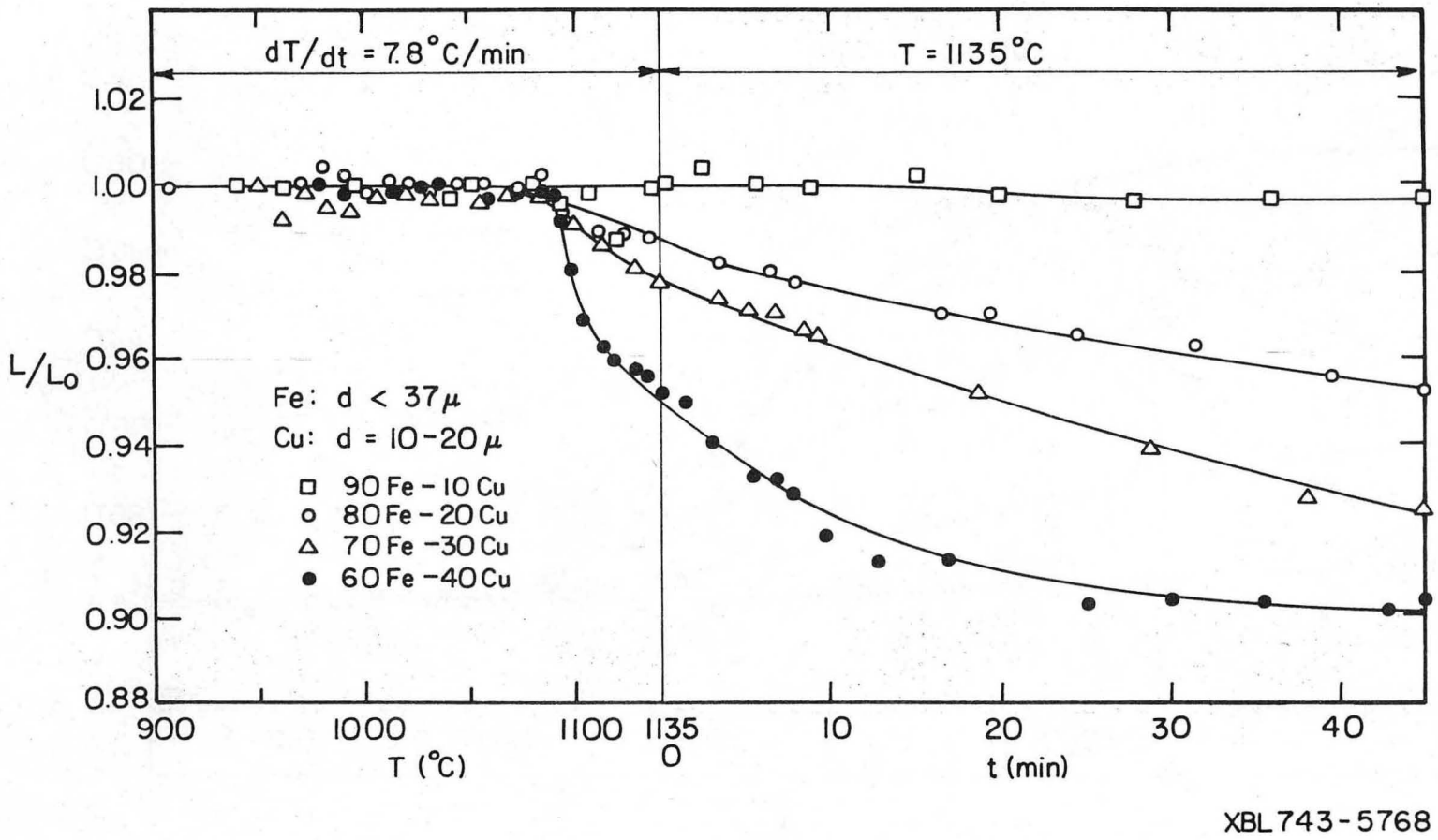
dT/dt = 7.8°C/min
T = 1135°C
1.02
1.00
0.98
0.96
0.94
0.92
0.90
0.88
L/Lo
Fe: d < 37μ
Cu: d = 10-20μ
90 Fe - 10 Cu
80 Fe - 20 Cu
70 Fe -30 Cu
60 Fe -40 Cu
900
1000
1100
1135
T (°C)
0
10
20
30
40
t (min)
XBL 743-5768

Fig. 5

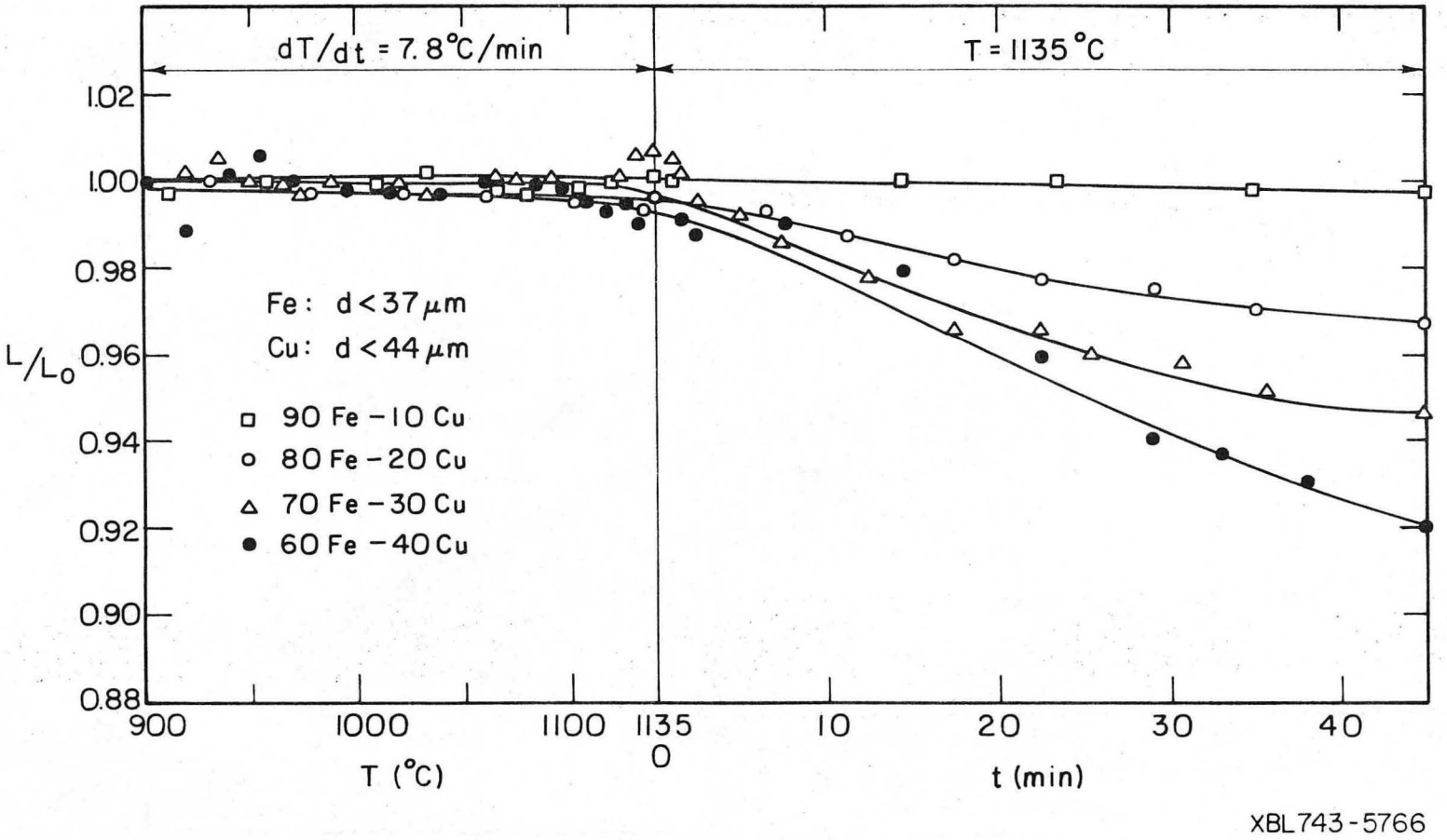
dT/dt = 7.8°C/min
T = 1135°C
1.02
1.00
0.98
0.96
0.94
0.92
0.90
0.88
L/L0
Fe: d<37μm
Cu: d<44μm
90 Fe - 10 Cu
80 Fe - 20 Cu
70 Fe - 30 Cu
60 Fe - 40 Cu
900
1000
1100
1135
0
10
20
30
40
T (°C)
t (min)
XBL743-5766

Fig. 6

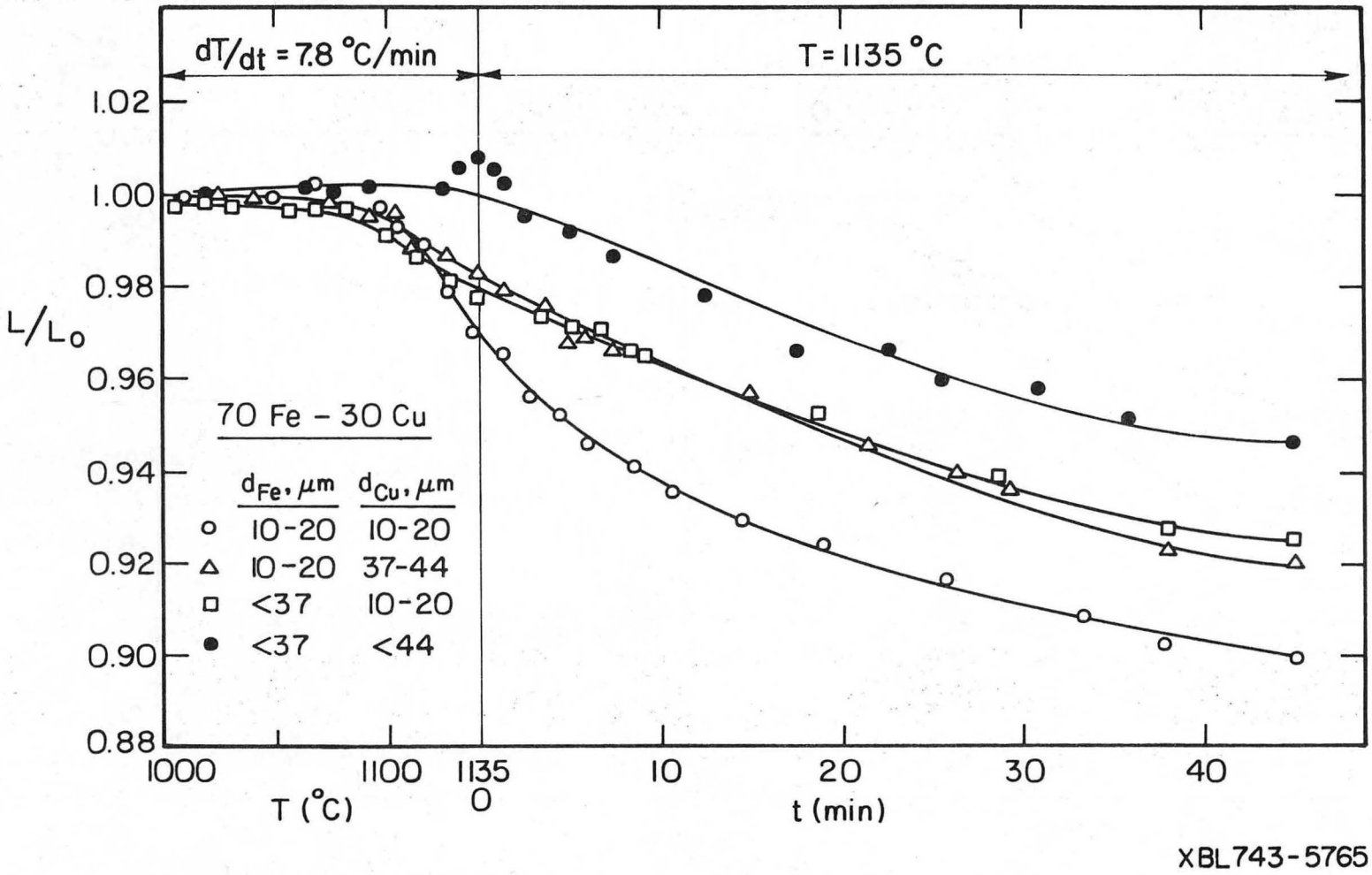
dT/dt = 7.8 °C/min
T = 1135 °C
1.02
1.00
0.98
0.96
0.94
0.92
0.90
0.88
L/Lo
70 Fe – 30 Cu
dFe, μm
dCu, μm
10-20
10-20
10-20
37-44
<37
10-20
<37
<44
1000
1100
1135
T (°C)
0
10
20
30
40
t (min)
XBL743-5765

Fig. 7

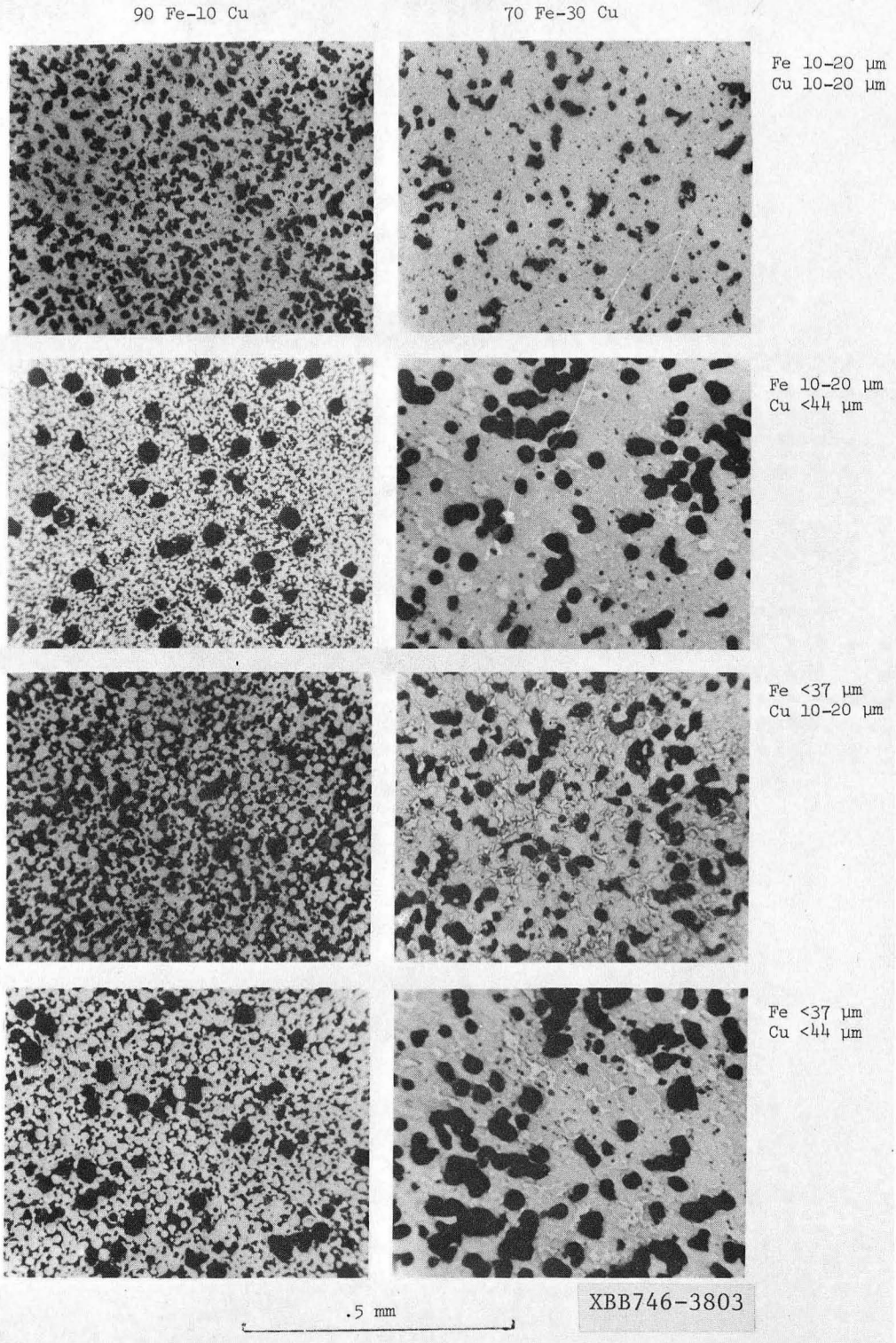
90 Fe-10 Cu
70 Fe-30 Cu
Fe 10-20 μm
Cu 10-20 μm
Fe 10-20 μm
Cu <44 μm
Fe <37 μm
Cu 10-20 μm
Fe <37 μm
Cu <44 μm
.5 mm
XBB746-3803

Fig. 8

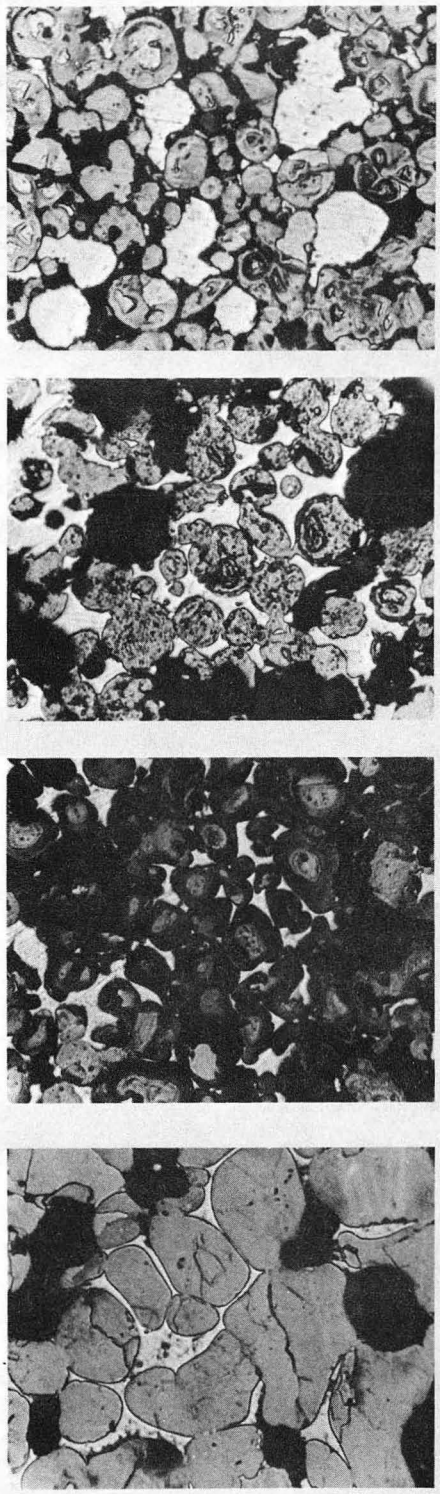

XBB746-3802

Fig. 9

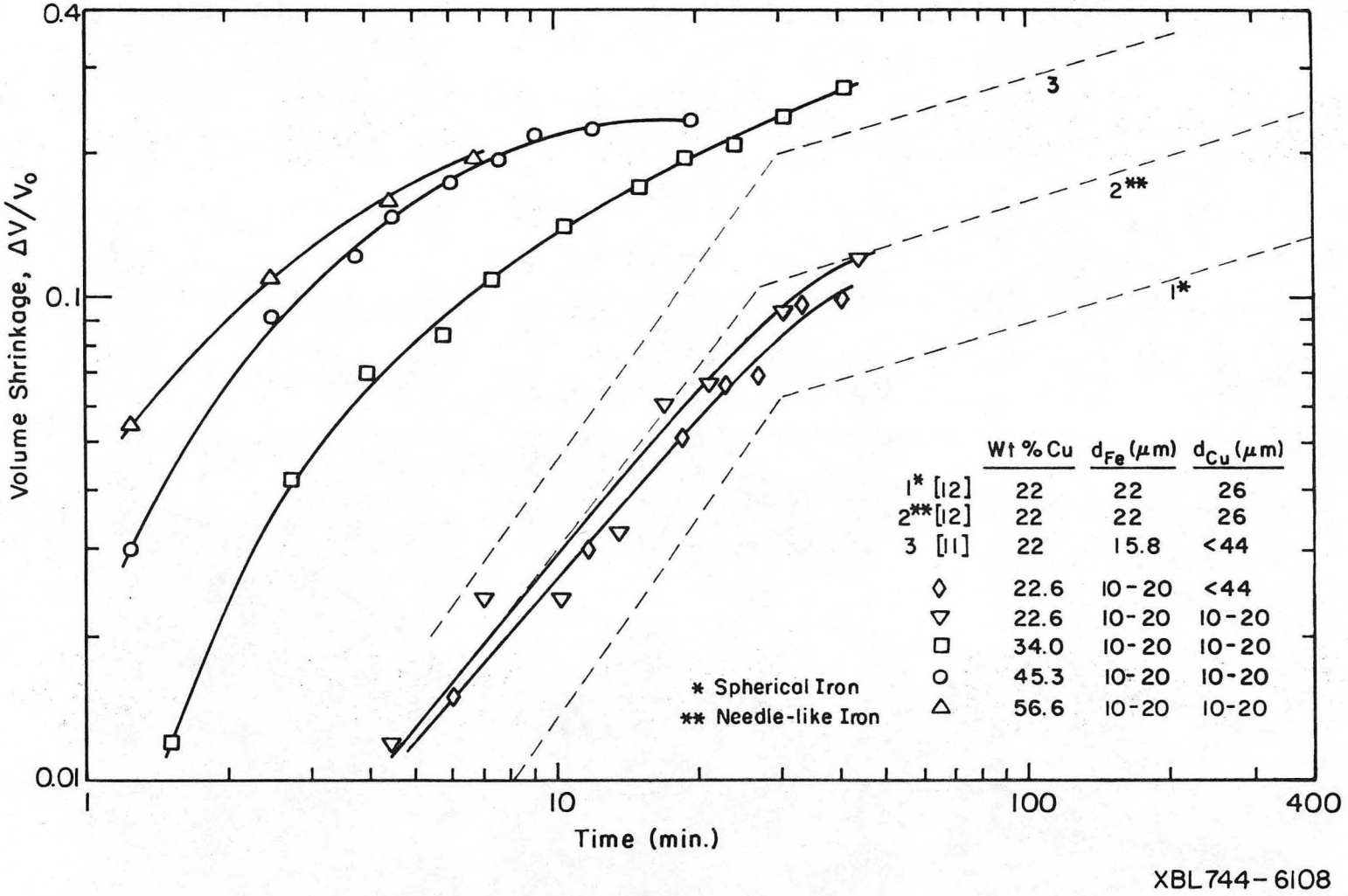
0.4
0.1
0.01
Volume Shrinkage, ΔV/V₀
1
10
100
400
Time (min.)
3
2**
1*
Wt % Cu
d_Fe (μm)
d_Cu (μm)
1* [12] 22 22 26
2** [12] 22 22 26
3 [11] 22 15.8 <44
◇ 22.6 10-20 <44
▽ 22.6 10-20 10-20
□ 34.0 10-20 10-20
○ 45.3 10-20 10-20
△ 56.6 10-20 10-20
* Spherical Iron
** Needle-like Iron
XBL744-6108

Fig. 10

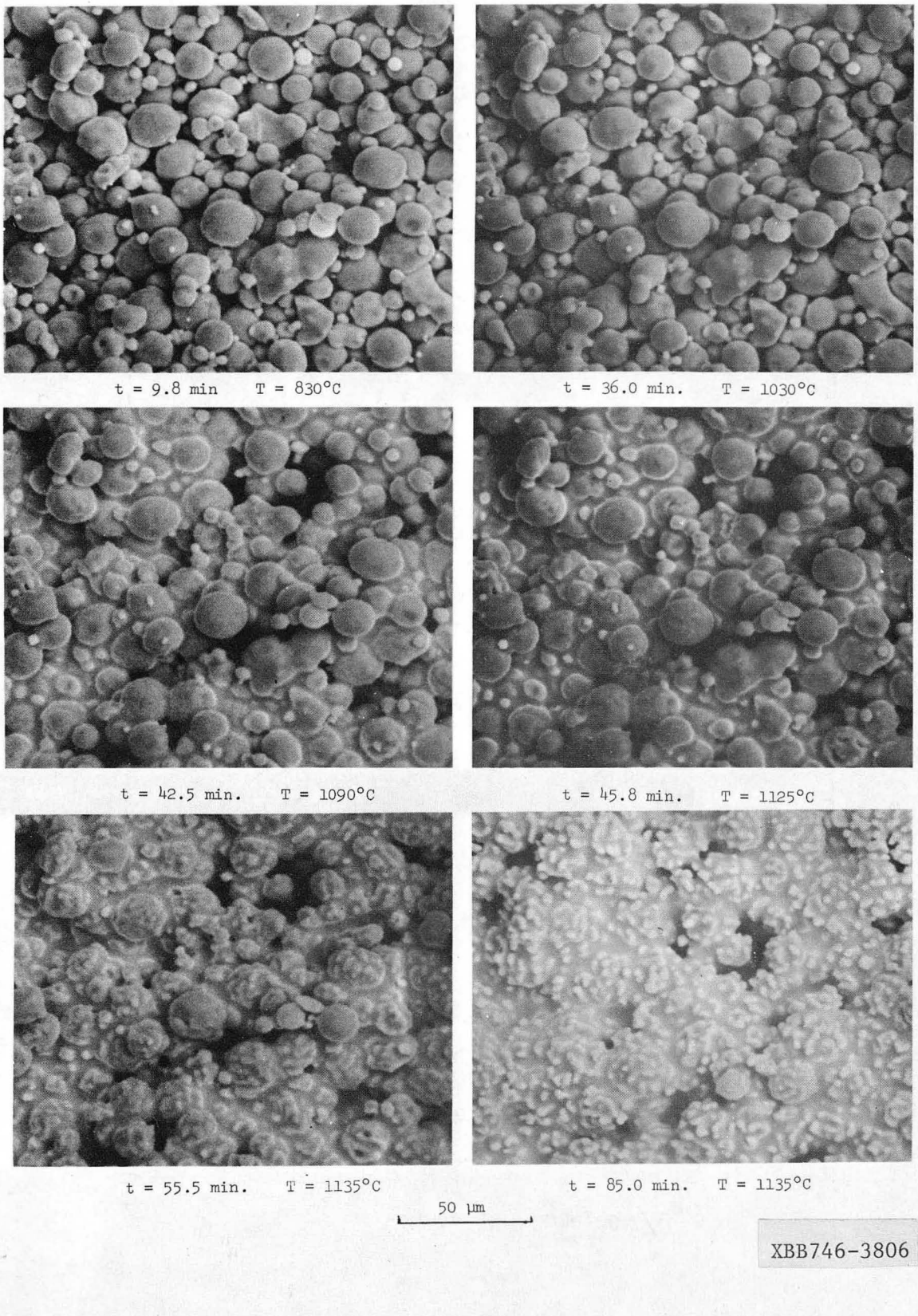
t = 9.8 min T = 830°C
t = 36.0 min. T = 1030°C
t = 42.5 min. T = 1090°C
t = 45.8 min. T = 1125°C
t = 55.5 min. T = 1135°C
t = 85.0 min. T = 1135°C
50 µm
XBB746-3806

Fig. 11

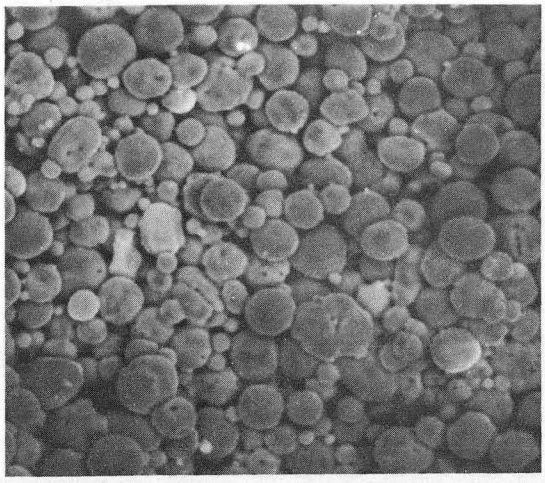

t = 6.5 min. T = 900°C

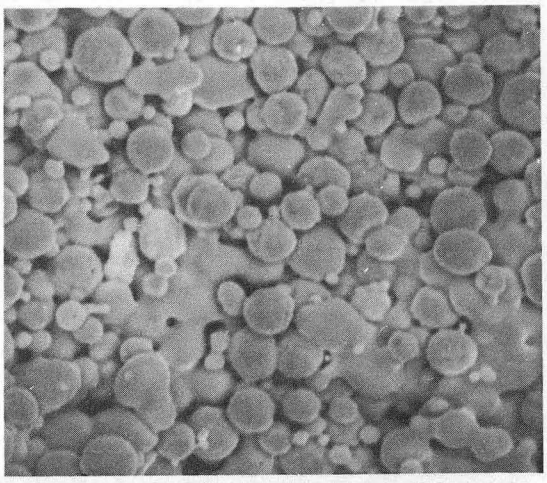

t = 35.2 min T = 1080°C

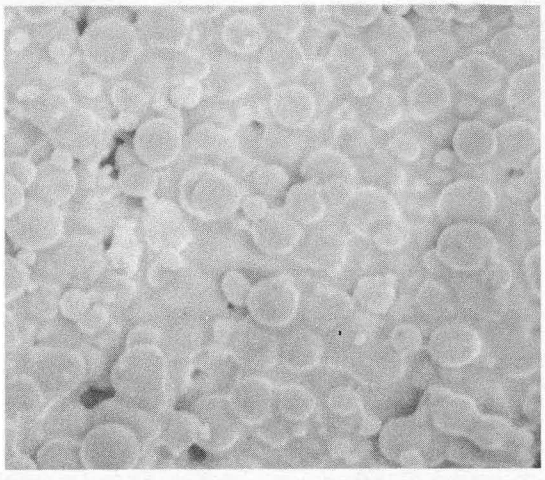

t = 36.0 min. T = 1090°C

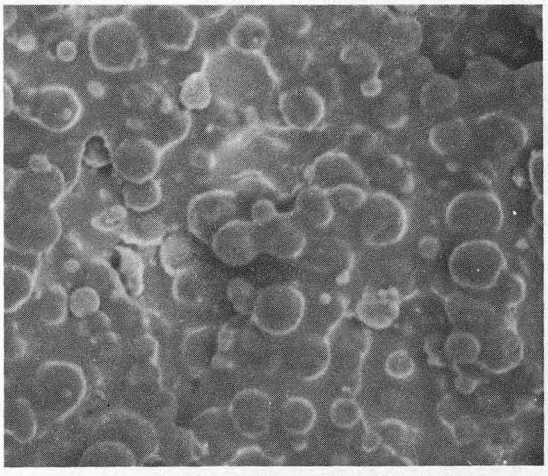

t = 37.8 min. T = 1105°C

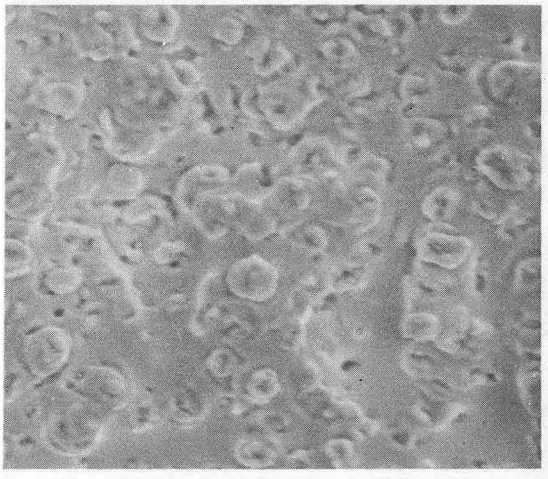

t = 46.6 min. T = 1135°C

50 µm

XBB746-3805

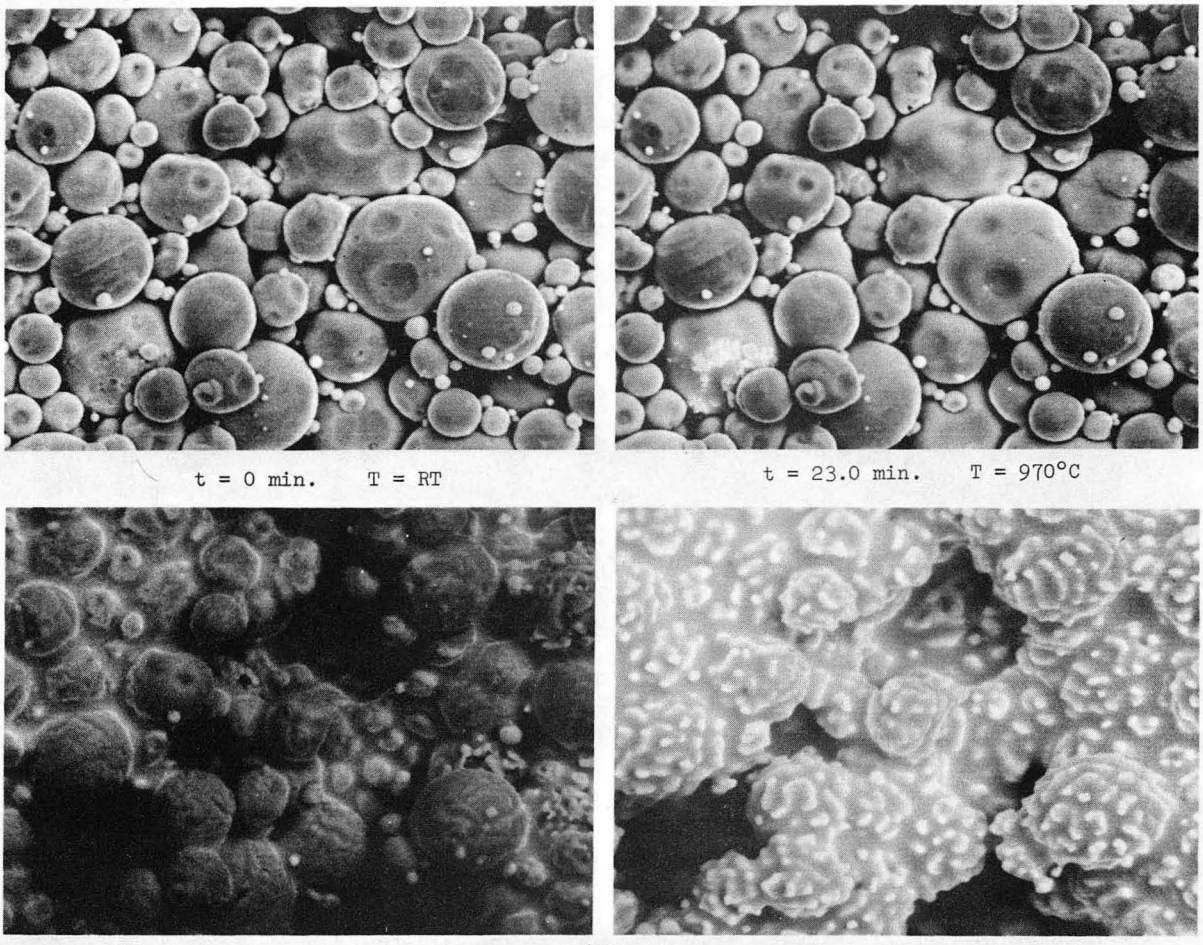
t = 0 min. T = RT
t = 23.0 min. T = 970°C
t = 42.7 min. T = 1135°C
t = 72 min. T = 1135°C
100 µm
XBB746-3804

Fig. 13

TECHNICAL INFORMATION DIVISION
LAWRENCE BERKELEY LABORATORY
UNIVERSITY OF CALIFORNIA
BERKELEY, CALIFORNIA 94720